Wave Exchange between the Ground Surface and a Boundary-Layer Critical Level

CARMEN J. NAPPO

Air Resources Laboratory, National Oceanic and Atmospheric Administration, Atmospheric Turbulence and Diffusion Division, Oak Ridge, Tennessee

GEORGE CHIMONAS

School of Geophysical Sciences, Georgia Institute of Technology, Atlanta, Georgia

(Manuscript received 17 December 1990, in final form 21 August 1991)

ABSTRACT

Gravity waves induced by two- and three-dimensional terrain features are examined theoretically in the planetary boundary layer (PBL) using a linear wave model that includes reabsorption at a critical level. The PBL structure is characterized by a constant Brunt–Väisälä frequency and a hyperbolic tangent wind speed profile, which can be adjusted to produce critical levels. It is found that for typical values of wind speed and thermal stratification in the stable PBL and for even mild terrain disturbances, the Reynolds stress and surface drag caused by surface-generated waves can be at least as large as those conventionally associated with surface friction. The wave drag will act on the PBL flow where wave dissipation occurs, for example, at a critical level or in regions of wave breaking. The drag over a given crosswind section of a two-dimensional ridge is about twice as great as that over a three-dimensional hill of approximately the same horizontal area. An entirely new result is the prediction that over a three-dimensional hill the wave stresses may generate a horizontal layer of counterrotating vortices immediately below a critical level.

1. Introduction

The parameterization of the flux of atmospheric momentum to the ground surface is among the important objectives of boundary-layer meteorology. Conventional boundary-layer theory is concerned mainly with the vertical transport of momentum by turbulence. However, it has been shown (Chimonas and Nappo 1989) that internal gravity waves generated by gentle surface irregularities also transport significant amounts of atmospheric momentum to the ground surface. The purpose of this paper is to evaluate the magnitude of this wave-generated stress relative to the turbulence-generated stress when the PBL flow absorbs the wave at a critical level. Some associated peculiarities of such flows in the case of waves generated by three-dimensional hills are also examined.

Many papers have been published on the subject of gravity waves in the atmosphere; however, only a small percentage of these have been directed toward gravity waves in the boundary layer, and almost no attention has been paid to the role they may play in the dynamics of the boundary-layer mean flow (but see Hines 1970).

Sawyer (1959) recognized that the generation of gravity waves by a mountain requires a transfer of momentum from the atmosphere to the ground surface. This extraction of momentum should then act much like a frictional stress somewhere on the atmospheric flow. Sawyer assumed that about half of the wave drag would be exerted on the lowest 3 km of the atmosphere, and the remainder would be distributed over the upper troposphere and stratosphere. Subsequently, Eliassen and Palm (1960) showed that unless these mountain waves are absorbed they will transfer momentum vertically at a constant rate; that is, the Reynolds stresses associated with each wave will be constant. Obviously, if the wave stress is to have an effect on the atmosphere, the waves and the momentum they carry must be absorbed by the mean flow. Booker and Bretherton (1967) showed that, according to linear wave theory, when a wave passes through a level where the horizontal phase velocity of the wave equals the background wind speed, the wave Reynolds stress is reduced by a factor $\exp[-2\pi(R_c - 0.25)^{1/2}]$, where R_c is the local Richardson number. If R_c is unity or larger, this is a substantial reduction; for example, 4×10^{-3} when $R_c = 1$ and 5×10^{-6} when $R_c = 4$. Such a convergence of the Reynolds stress across the "critical level" would allow the wave drag generated at the ground surface to act on the atmosphere.

How, or indeed whether, the wave momentum is transferred to the mean flow at the critical level is not certain. The linear wave theory suggests that the Reynolds stress is reduced there. However, the theory also

Corresponding author address: Dr. Carmen Nappo, Air Resources Laboratory, NOAA/ERL, 456 S. Illinois Ave., P.O. Box 2456, Oak Ridge, TN 37830.

predicts that as the wave approaches a critical level ($z \rightarrow z_c$), the horizontal velocity perturbation grows as $(z_c - z)^{-1/2}$, where z_c is the height of the critical level and z is the height of the wave above the ground surface; eventually, the velocity perturbation becomes so large that the linear theory ceases to apply. It is assumed that the wave becomes unstable and breaks down into turbulence in the vicinity of the critical level.

Because the mountain waves are stationary, their horizontal phase velocities are necessarily zero. Critical levels for these waves will exist wherever the component of the background wind in the direction of wave propagation reverses direction. The basis of the research described in this paper is that identical processes occur in the stable planetary boundary layer; only the scales of the problem will differ. For the mountain wave problem, the horizontal and vertical length scales are typically 10 km and 1 km, respectively; for the surface-generated wave in the PBL, the horizontal and vertical length scales are more likely 1000 m and 100 m, respectively. The vertical displacements of air parcels by these waves in the PBL will be quite small in comparison to those generated by mountains; however, these boundary-layer waves and their associated stress are as important on the PBL scale as the mountain waves are on the global scale.

Only a few studies have been made of vertically propagating gravity waves launched by three-dimensional obstacles. Blumen (1965) calculated the wave-generated momentum flux and surface drag for a rotating atmosphere. Bretherton (1969) calculated the momentum transport by gravity waves launched from a 90-km-square region in North Wales. Blumen and McGregor (1976) examined the effects of crosswind and vertical shear on wave drag over a three-dimensional hill. Smith (1980) looked at several aspects of the flow structure over a mountain, including the near and far fields, the breakdown of linear theory, the criterion for flow around the mountain, and the effects of nonhydrostatic flow. Simard and Peltier (1982) calculated the perturbation flow fields produced by isolated islands in the Norwegian and Barents seas; also, their model included critical levels. Hines (1988) developed analytical expressions for the wave drag and average Reynolds stress for the case of uniform, hydrostatic flow over a mountain. Lin and Li (1988) used linear theory to examine the three-dimensional response of a shear flow to elevated heating resulting in thermally forced gravity waves. All of these studies are cast in terms of disturbances on the tropospheric scale. On the PBL scale, a majority of the terrain disturbances are three-dimensional, for example, bluffs, buttes, hills, and broken ridges; thus, it can be expected that the wave perturbations generated by these obstacles will be an important part of the PBL dynamics.

The wave–turbulence processes discussed above have no simple counterpart over flat terrain, yet almost all studies of turbulence in the PBL have been made over nearly flat surfaces (Businger et al. 1971; Clarke et al. 1971; Izumi and Caughey 1973; Kondo et al. 1978; Yamamoto et al. 1979; Mahrt et al. 1979; Garratt 1983). From these observations, flux–profile relationships have been developed that formed the basis for model studies (see, for example, Delage 1974; Wyngaard 1975; Brost and Wyngaard 1978; Rao and Snodgrass 1979). Basic to these studies is the assumption that the upper-level flow does not directly sense the presence of the ground surface (Nieuwstadt 1984). However, there are few truly flat ground surfaces of significant extent in nature. Even small undulations in terrain elevation generate gravity waves that lead to Reynolds stresses not accounted for in these flux-profile formulations. Current PBL parameterizations underestimate the momentum flux over regions of even moderately complex terrain (Chimonas and Nappo 1989).

In the absence of critical levels, wave dissipation is quite weak, so if waves are to significantly affect the mean state of the PBL, critical levels are probably essential. Critical levels occur where the component of the background wind in the plane of the wave vanishes, that is, where this component reverses direction. Over regions of complex terrain, wind reversals within the PBL are quite common. Above sloping terrains, downslope drainage winds with an upslope return wind aloft are often observed (see, for example, Hootman and Blumen 1983; Clements et al. 1989). Figure 1, taken from Mahrt (1985), shows the wind and temperature fields in the PBL constructed from instrumented aircraft flights over moderately complex terrain in central Oklahoma. During these flights, a northerly surface flow undercut a less stable southerly flow. It is interesting to note in Fig. 1 that regions of high turbulence as measured by the vertical velocity variance are concentrated in regions of wind reversals. The above examples represent wind reversals in two-dimensional flows; however, when the horizontal wind direction varies strongly with height, it is possible that an azimuthal component of the surface wind normal to a terrain feature will reverse its direction somewhere aloft.

Over flat uniform terrain, wind reversals within the PBL are unlikely, but over flat terrain surface-generated gravity waves are also unlikely. There are many concentrations of population and industry in regions with complex terrain. Thus, the present study is relevant especially if more reliable models of complex terrain flow fields are to be developed.

2. Mathematical framework and model equations

a. The wave equations

The starting point in the analysis is the Taylor–Goldstein equation (Gossard and Hooke 1975), which describes the propagation of gravity waves [see Smith

(1979) for a detailed discussion of mountain waves]. Assuming horizontally uniform and steady background flow, $U(z)$, the Taylor–Goldstein equation for waves generated by a two-dimensional ridge is

$$\hat{w}_{zz} + \left[\frac{N^2}{U^2} - \frac{U_{zz}}{U} - k^2\right]\hat{w} = 0, \quad (2.1)$$

where $\hat{w}(k, z)$ is the Fourier transform of the wave-perturbation vertical velocity, N the Brunt–Väisälä frequency, k the horizontal wavenumber, and subscript z the vertical derivative. The Brunt–Väisälä frequency is given by

$$N^2 = \frac{g}{\theta_0}\frac{\partial \theta_0}{\partial z}, \quad (2.2)$$

where g is the acceleration of gravity, θ the potential temperature, and θ_0 its unperturbed value. It is understood that U is directed normal to the ridge line, and the flow is in the positive x direction. The vertical velocity in physical space is given by

$$w(x, z) = \frac{1}{2\pi}\int_{-\infty}^{\infty} \hat{w}(k, z)e^{ikx}dk. \quad (2.3)$$

It is useful to introduce a nondimensional shape function $\phi(k, z)$ defined by

$$\hat{w}(k, z) = ikU_0\hat{h}(k)\phi(k, z), \quad (2.4)$$

where $U_0 = U(z = 0)$, and $\hat{h}(k)$ is the Fourier transform of the terrain height profile, that is,

$$\hat{h}(k) = \int_{-\infty}^{\infty} h(x)e^{-ikx}dx. \quad (2.5)$$

At the bottom boundary, we require $\phi(k, 0) = 1$, which renders the kinematic boundary condition for $\hat{w}$. At the top of the model, we impose the radiation condition on ϕ; that is, only upward propagation of energy is allowed.

For the case of flow over a three-dimensional hill, the Taylor–Goldstein equation is

$$\hat{w}_{zz} + \left[\frac{(k^2 + l^2)N^2}{(kU + lV)^2} - \frac{(kU_{zz} + lV_{zz})}{kU + lV} - (k^2 + l^2)\right]\hat{w} = 0, \quad (2.6)$$

where V is the background velocity component and l is the wavenumber in the y direction. A shape parameter $\Phi(k, l, z)$ defined by

$$\hat{w}(k, l, z) = i(kU_0 + lV_0)\hat{h}(k, l)\Phi(k, l, z) \quad (2.7)$$

is introduced, where $V_0 = V(z = 0)$ and

$$\hat{h}(k, l) = \int_{-\infty}^{\infty}\int_{-\infty}^{\infty} h(x, y)e^{-i(kx+ly)}dxdy. \quad (2.8)$$

At the bottom boundary we require $\Phi(k, l, 0) = 1$, and at the top boundary impose the radiation condition on Φ. The wave amplitudes of the horizontal perturbation velocities are given by

$$\hat{u}(k, l, z) = \frac{ik}{k^2 + l^2}\left[\frac{\hat{w}l(lU_z - kV_z)}{k(kU + lV)} + \frac{\partial \hat{w}}{\partial z}\right] \quad (2.9a)$$

$$\hat{v}(k, l, z) = \frac{-il}{k^2 + l^2}\left[\frac{\hat{w}k(lU_z - kV_z)}{l(kU + lV)} - \frac{\partial \hat{w}}{\partial z}\right]. \quad (2.9b)$$

Note that by setting $l = 0$ in (2.9a, b), the solutions for the two-dimensional ridge problem are obtained.

A nondimensional form of (2.1) is obtained by introducing the dimensionless variables

$$U_* = U/U_0, \quad z_* = z/H$$
$$k_* = kH, \quad N_* = NH/U_0, \quad (2.10)$$

where H is the maximum ridge height. Then (2.1) along with (2.4) becomes

$$\phi_{zz} + \left[\frac{F^{-2}}{U_*^2} - \frac{1}{U_*}\frac{\partial^2 U_*}{\partial z_*^2} - k_*^2\right]\phi = 0, \quad (2.11)$$

where $F = U_0/NH$ is the Froude number.

b. *Wave drag*

The drag per unit crosswind direction over a two-dimensional ridge, D, is obtained by integrating the Reynolds stress at the ground surface over all x,

$$D = \int_{-\infty}^{\infty} -\bar{\rho}uwdx = \int_0^{\infty} \frac{-\bar{\rho}}{\pi}[U_0\hat{h}(k)]^2k \times \mathrm{Im}\left[\phi(k, 0)\frac{d}{dz}\phi^*(k, 0)\right]dk, \quad (2.12)$$

where $\bar{\rho}$ is the average PBL air density, an asterisk represents the complex conjugate value, and Im[ ] selects the imaginary part of the expression in braces. In the absence of wave dissipation, the wave Reynolds stress is constant with height; however, at a critical level where wave absorption occurs, the stress acts on the mean flow. This provides the fluid deceleration that is the reaction to the drag exerted by the mean flow at the surface. While details of wave absorption are not contained in linear theory, the response of the mean flow can be estimated with a simplified analysis. Let the wave be absorbed over a distance δ below the critical level. The deceleration of the layer of fluid that absorbs the stress obeys

$$-\bar{\rho}\delta\int_{-\infty}^{\infty}\frac{DU_2}{Dt}dx = D, \quad (2.13)$$

where U_2 is a second-order perturbation flow generated by the first-order wave perturbations (Booker and Bretherton 1967). The advective term is approximated in the mean by the zero-order advection associated with the mean field U, so

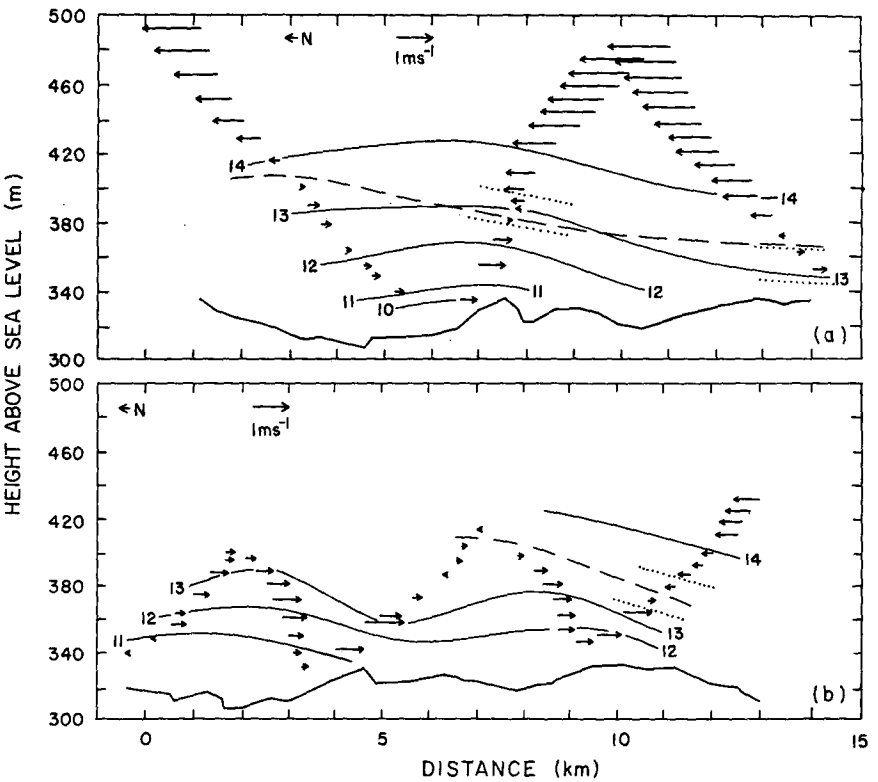

FIG. 1. Two cross sections of low-level airflow constructed from aircraft data taken with two similar undulating flight tracks (Mahrt 1985). Lower solid line marks the terrain surface. Potential temperature (°C, solid lines); dotted lines enclose regions of vertical velocity variance greater than 0.01 $m^2 s^{-2}$.

$$\frac{D}{Dt} \approx U \frac{\partial}{\partial x},$$

and the total change of flow across the ridge, ΔU_2, becomes

$$\Delta U_2 = \int_{-\infty}^{\infty} \frac{\partial U_2}{\partial x} dx = -D/(\bar{\rho}\delta U). \quad (2.14)$$

The appropriate value to associate with U is the mean speed of the fluid layer that does the absorbing, say $U(z_c - \delta/2) = U_a$. However, it is now seen from (2.14) that if $(D/\bar{\rho}\delta) \geqslant U_a^2$, then the second-order flow builds to the point where it is equal and opposite to the zero-order mean flow, at which point continued passage across the ridge ceases. In the sense described by Hines (1988), we take this to be a blocking condition. Because $U(z_c) = 0$, the nearby value U_a can be expected to be small, making blocking likely for quite moderate values of the drag D.

Over a three-dimensional hill, the Reynolds stress in the along-wind direction, τ_x and in the crosswind direction, τ_y, are given by

$$\tau_x(x, y, z) = -\bar{\rho}u(x, y, z)w(x, y, z)$$
$$\tau_y(x, y, z) = -\bar{\rho}v(x, y, z)w(x, y, z). \quad (2.15)$$

For the case of flow over a symmetric hill, $v(x, y, z) = -v(x, -y, z)$; hence, the drag components are

$$D_x = -\bar{\rho} \int_{-\infty}^{\infty} dy \int_{-\infty}^{\infty} uwdx$$
$$D_y = 0. \quad (2.16)$$

c. *Wave-induced vorticity*

Over a three-dimensional obstacle, horizontal variations in the Reynolds stresses absorbed into the flow lead to the creation of mean vorticity. The process is illustrated in Fig. 2. Wave amplitudes, and hence Reynolds stress, maximize on the line of symmetry through the height profile and fall to zero at large distances from the obstacle. Since the horizontal layer of fluid that absorbs the stress is near a critical level and hence advects only at a very slow speed, the torques associated with the stress have time to cause a significant spinup of the fluid. The outcome of such generation of circulation appears to be the formation of a pair of counterrotating vortices, as depicted in Fig. 2. The process can be analyzed by equating the second-order terms in the wave-perturbation amplitude; the horizontal momentum equations yield

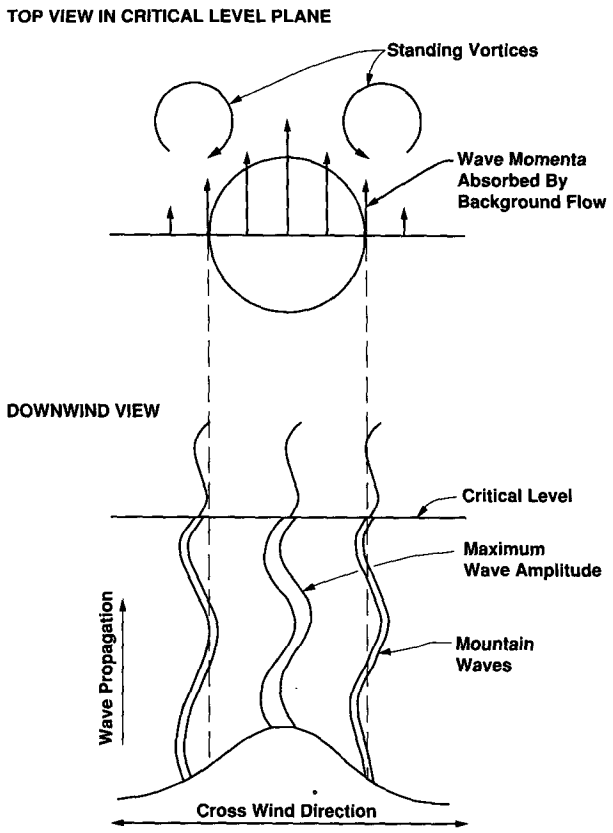

FIG. 2. Schematic illustration of wave-induced vorticity at a critical level above a three-dimensional hill.

$$\bar{\rho}\frac{DU_2}{Dt} = -\frac{\partial P_2}{\partial x} + \frac{\partial \tau_x}{\partial z} \tag{2.17}$$

and

$$\bar{\rho}\frac{DV_2}{Dt} = -\frac{\partial P_2}{\partial y} + \frac{\partial \tau_y}{\partial z}, \tag{2.18}$$

where some second-order wave-pressure gradients have been ignored. A similar equation is discussed by Booker and Bretherton (1967). An equation for the evolution of the vertical component of vorticity, ζ,

$$\zeta = \frac{\partial V_2}{\partial x} - \frac{\partial U_2}{\partial y}, \tag{2.19}$$

is now obtained from (2.17) and (2.18) as

$$\frac{D\zeta}{Dt} = \frac{1}{\bar{\rho}}\frac{\partial s}{\partial z}, \tag{2.20}$$

where

$$s = \frac{\partial \tau_y}{\partial x} - \frac{\partial \tau_x}{\partial y} \tag{2.21}$$

is the stress couple acting in the horizontal plane in the wave-absorbing layer. The simplest solution to (2.20) is obtained near a critical level where the horizontal wind speed is small. In this case, (2.20) is approximately

$$\frac{\partial \zeta}{\partial t} = \frac{1}{\bar{\rho}}\frac{\partial s}{\partial z}. \tag{2.22}$$

Because the wave stresses are time-independent, (2.22) can be immediately integrated to yield

$$\zeta = \frac{1}{\bar{\rho}}\frac{\partial s}{\partial z}(t - t_0), \tag{2.23}$$

where t_0 is the time at which the upward propagating gravity waves first reach that height near the critical level where absorption begins. If this absorption is taken to be complete over a distance δ below the critical level, then the perturbation vorticity is

$$\zeta = -\frac{s}{\bar{\rho}\delta}(t - t_0), \tag{2.24}$$

where s is evaluated at distance δ below the critical level. In this case, the perturbation vorticity is predicted to increase linearly with time, but this can only continue as long as the total mean state maintains the conditions that allow wave absorption without significant advection of vorticity out of the region.

d. The critical level

The mathematical treatment of critical levels in atmospheric dynamics is presented by Booker and Bretherton (1967), who follow an analysis given by Miles (1961). Detailed descriptions of the computational techniques for integrating the Taylor–Goldstein equation across the singularity at the critical level can be found in, for example, Lalas and Einaudi (1976), Simard and Peltier (1982), Craik (1985), and Nappo (1989). A brief description of the technique is given in the Appendix.

e. The model parameters

The two-dimensional ridge is modeled by a Gaussian distribution

$$h(x) = He^{-x^2/b^2}, \tag{2.25}$$

where H is the maximum elevation of the ridge and b is the scale of the ridge width. The half-width of the ridge is given by $0.83b$. The finite Fourier transform of $h(x)$ over the interval $-L \leq x \leq L$ is

$$\hat{h}(k_n) = \frac{Hb\sqrt{\pi}}{2L}e^{-k_n^2 b^2/4} + \mathrm{O}\left(e^{-L^2/b^2}\frac{H}{k_n L}\right), \tag{2.26}$$

where L is chosen large enough to include all the important features of the disturbed flow and all the effective displacement associated with the ridge so that the correction O( ) in (2.26) can be ignored. We find that the finite Fourier series converge in a satisfactory

way with $L/b = 20$. The three-dimensional isotropic hill is also Gaussian,

$$h(x, y) = H_G e^{-(x^2+y^2)b^2}, \tag{2.27}$$

with Fourier transform

$$\hat{h}(k_n, l_m) = \frac{H_G b^2 \pi}{4L^2} e^{-(k_n^2+l_m^2)b^2/4} + \mathrm{O}\left(e^{-L^2/b^2} \frac{H}{\sqrt{n^2+m^2}}\right). \tag{2.28}$$

The background wind $\mathbf{V} = \hat{x}U(z)$ is modeled by a hyperbolic tangent profile

$$2U(z) = (U_B + U_T) - (U_B - U_T)\tanh[(z - z_i)/z_s]. \tag{2.29}$$

The inflection point, z_i, is fixed at 200 m above the ground surface, $z = 0$, and the scale of the wind shear, z_s, is fixed at 50 m. Accordingly, the ground-level wind speed, $U(0)$, is essentially U_B, while for all heights above 300 m, the wind is very close to the constant value U_T. Note that when U_B and U_T are of opposite sign, a critical level exists. For most of the calculations, the background thermal stability is held constant at 0.025 K m^{-1}, which gives a Brunt–Väisälä frequency of 0.03 s^{-1}. The upper boundary of the model is set at 1000 m.

The wavenumbers used in the calculations are given by

$$k_n = \frac{n\pi}{L} = \frac{n\pi}{20b}, \tag{2.30}$$

where the maximum value of integer n is 50, which makes the smallest Fourier wavelength, λ_{50}, equal to $0.8b$. This truncated spectrum includes all the Reynolds stress, since examination of (2.12) and (2.26) shows that the stress spectrum peaks at wavenumber k such that $(kb/2)^2 = 1$ and then falls off exponentially as $e^{-(kb/2)^2}$. Thus, by wavenumber 50 the Gaussian has fallen to 10^{-6} of its peak value and this, and higher, wavenumbers are not significant in the drag computations.

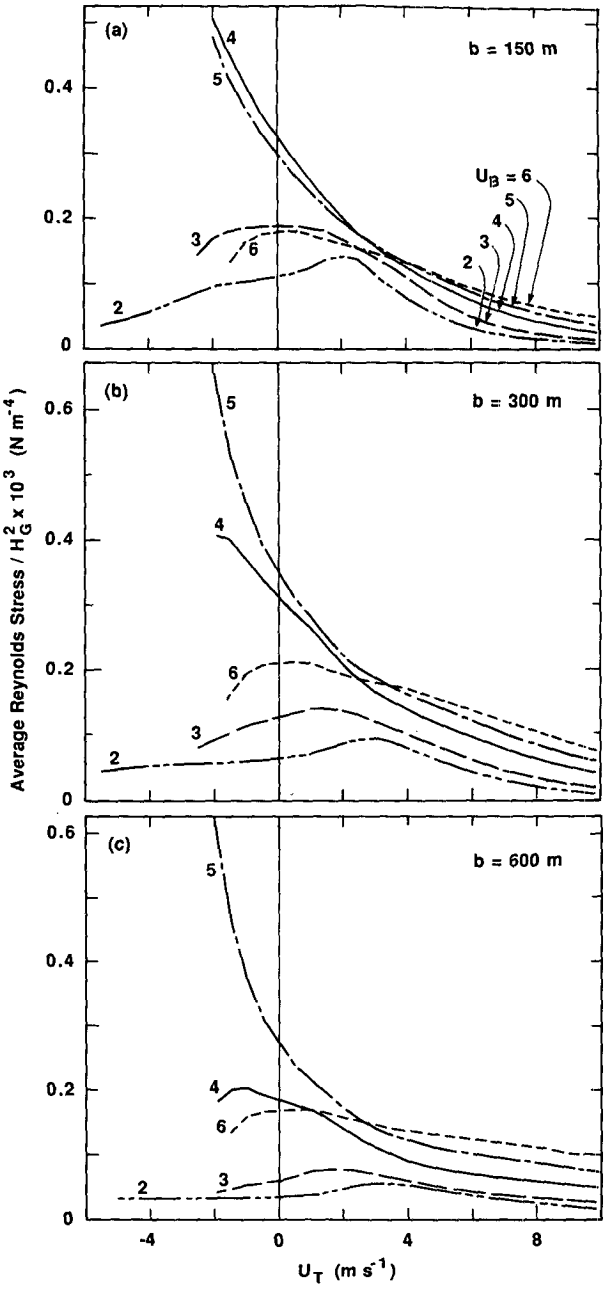

FIG. 3. Average Reynolds stress above a two-dimensional Gaussian-shaped ridge as a function of upper-level wind speed, U_T, for five values of lower-level wind speed, U_B. Values are normalized by the square of the maximum ridge height.

3. Results

a. Two-dimensional ridge

The wave drag per unit length of ridge, D, was examined by Chimonas and Nappo (1989) for the special case when no critical levels are present in the PBL. In Fig. 3, we plot the curves of average Reynolds stress over a ridge when critical levels are allowed. Three ridge widths are considered: b = 150, 300, and 600 m; U_B is the wind speed at the bottom boundary, and U_T is the wind speed at the top boundary. The average stress is obtained by dividing D by $2.54b$, which is the width of the ridge at height $0.2H$. The terminations of these curves in the negative U_T regions of the graphs mark the points where the Richardson number at the critical level becomes less than 1/4. The curves pass smoothly through $U_T = 0$, which divides the critical and noncritical level regimes. The wave stress is seen to be a complicated function of the wind structure, that is, U_B

and U_T. Wave stress generally decreases with increasing ridge width, but this is not a significant effect. It is apparent from Fig. 3 that for sufficiently wide ridges, the wave stress approaches a constant value for small values of U_B when a critical level is present, for example, when $b = 300$ m and $U_B = 2$ m s^{-1}. In these instances, an acceptable estimate of the wave drag can be obtained by setting U_T to a small positive value, thus avoiding the need to consider the critical level. However, this is generally not possible, for example, when $U_B = 5$ m s^{-1}.

The average Reynolds stress as a function of U_B for the three different ridge widths is plotted in Fig. 4 for the case when $U_T = -1$ m s^{-1}. The stresses over the three ridge sizes are not greatly different. More interesting is the tendency for the stress maxima to occur at about the same values of U_B. This behavior is also seen when critical levels are not present (see, for example, Fig. 7 of Chimonas and Nappo 1989). We attribute this behavior to the background wind structure. The Scorer parameter, l_s^2, defined as

$$l_s^2 = \frac{N^2}{U^2} - \frac{U_{zz}}{U}, \tag{3.1}$$

partitions the gravity waves into external type, $l_s^2 < k^2$, and internal type, $l_s^2 > k^2$. Whenever l_s^2 decreases with height, some waves will change from internal to external type waves. External waves cannot propagate momentum vertically; however, if the external wave changes back into an internal wave, it will again propagate momentum upward, but at a reduced value. Figure 5 shows vertical profiles of l_s^2 for various values of U_B with $U_T = -1$ m s^{-1}. As the critical level is approached, $U(z \to z_c) \to 0$ and $l_s^2 \to \infty$. For U_B greater than about 4 m s^{-1}, l_s^2 decreases with height below the critical level and the high wavenumber gravity waves switch to external waves. As U_B increases in value, more of the waves become external. However, because l_s^2 becomes quite large near the critical level, all of the gravity waves must return to the internal type before they are absorbed, but they will have decreased amplitudes. Because of this the wave stresses reach maximum values at about the same values of U_B regardless of the ridge width, as shown in Fig. 4.

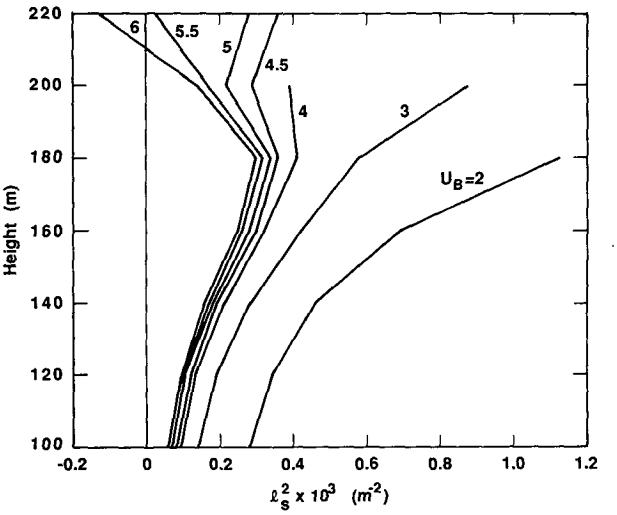

FIG. 5. Profiles of Scorer parameter for various values of surface wind speed U_B with constant $U_T = -1$ m s^{-1}.

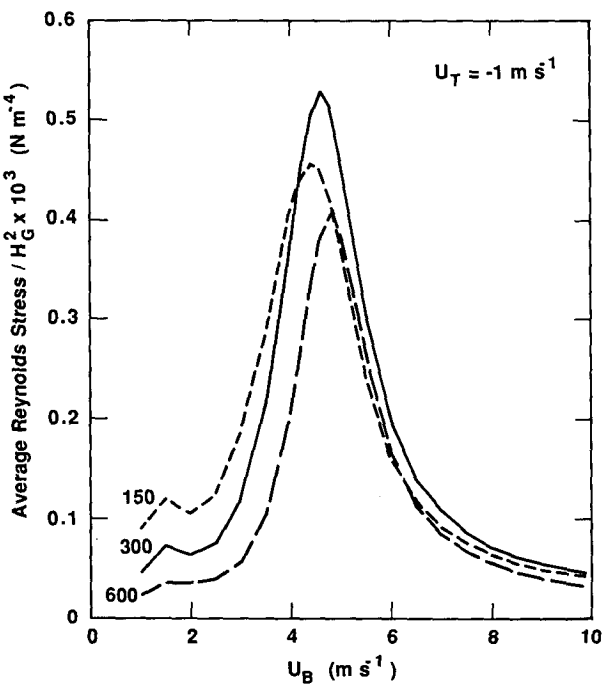

FIG. 4. Average Reynolds stress above a two-dimensional Gaussian-shaped ridge as a function of surface wind speed for various ridge widths.

To compare the relative magnitudes of wave stress and friction stress, we plot, in Fig. 6, the wave stress as a function of surface wind speed for three different values of N. The friction stress is given by $\frac{1}{2}\bar{\rho}C_D U_B^2$, where C_D is the aerodynamic drag coefficient; we use $C_D = 0.005$; also $b = 150$ m and $H = 15$ m. This is a gentle ridge with an aspect ratio $\alpha = H/(0.83b)$ of 0.12, yet for typical PBL conditions, the wave stress is as important as the friction stress.

In the hydrostatic limit, $Nb/U \gg 1$, Hines (1988) shows that, for the case of uniform wind speed, U, and constant Brunt–Väisälä frequency, N, the average Reynolds stress over a Gaussian-shaped ridge is given by

$$\tilde{\tau} = 0.4\bar{\rho}UH^2N/b. \tag{3.2}$$

If $\tilde{\tau}$ is expressed in terms of a drag coefficient for waves following Blumen and McGregor (1976), that is, $\tilde{\tau} = \frac{1}{2}\bar{\rho}C_{DW}U^2$, then

$$C_{DW} = 0.8NH^2/Ub = 0.66\alpha/F, \tag{3.3}$$

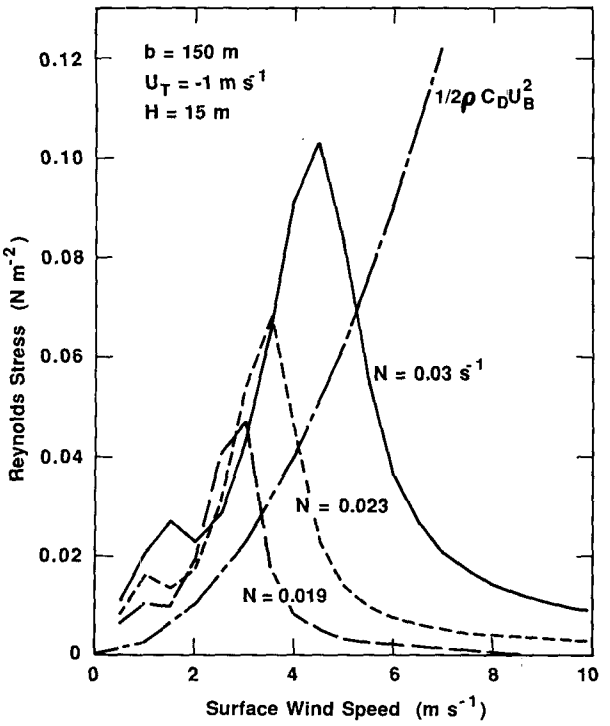

FIG. 6. Average Reynolds stress above a two-dimensional Gaussian-shaped ridge as a function of surface wind speed for various values of N. b = 150 m, $U_T = -1$ m s^{-1}, and H = 15 m. Also shown is the friction stress for C_D = 0.005.

where $F = U/NH$ is the Froude number. Unlike the surface drag coefficient, C_{DW} is not independent of wind speed. Typically, $\alpha \approx 0.06$ and $F \approx 10$ so that $C_{DW} = 0.005$, which is similar to typical values of surface drag coefficient.

A useful result is obtained if we perform our calculations in nondimensional space. In this case, (2.11) is used for the dimensionless wave solution. The nondimensional drag is obtained by using the dimensionless parameters (2.10) in (2.12). The dimensionless drag is then given by $D/\frac{1}{2}\bar{\rho}HU_B^2$. Curves of dimensionless wave drag are given in Fig. 7 for aspect ratios, α, of 0.06, 0.12, and 0.24, respectively. The curves in each graph are scaled by the inverse square of their respective Froude number $F^{-2} = (NH/U_B)^2$, and the terminations of these curves for $F^{-2} = 0.001$ and 0.01 mark the points where $R_c \leqslant 0.25$. For the same conditions leading to (3.2), Hines (1988) shows that the wave drag is $D = \bar{\rho}UH^2N$. Dividing this by $\frac{1}{2}\bar{\rho}HU^2$ gives the dimensionless wave drag

$$D_* = 2F^{-1}. \tag{3.4}$$

Thus, in the hydrostatic case, the dimensionless wave drag is constant. This is observed in Fig. 7 for $U_T/U_B < 1$ and $F^{-2} \geqslant 0.1$. It is also seen in Fig. 7 that the wave drag is maximum in the hydrostatic case.

b. *Wave breaking and flow blocking*

Where the horizontal velocity component of a standing wave is equal and opposite to the background wind speed, the flow streamlines become vertical and a blocking condition exists. Further increase in wave amplitude results in convective instability and wave breaking. Numerical simulations of airflow over mountains by Clark and Peltier (1977), Peltier and Clark (1979), Durran (1986), and Bachmeister and Pierrehumbert (1988) suggest that wave breaking leads to a reorganization of the flow field, resulting in severe downslope winds and large surface drag. Within the wave-breaking region a wave-induced critical layer is generated, and because the Richardson number is necessarily less than 1/4 (since this is a region of convective instability), wave reflection rather than wave absorp-

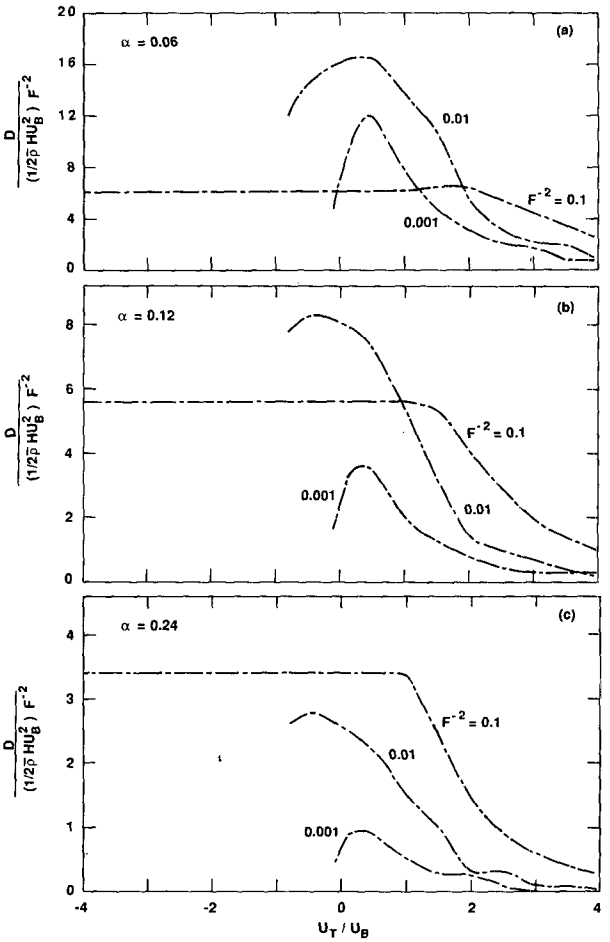

FIG. 7. Dimensionless wave drag above a two-dimensional Gaussian-shaped ridge as a function of dimensionless wind speed.

tion occurs. If this critical layer is near certain distinct heights, a resonance is established between the upward-propagating and downward-propagating reflected gravity waves. Wave breaking is an important process in the deep troposphere, and it is reasonable to expect that it is equally important in the boundary layer.

Wave breaking cannot be realized in a linear model since the wave fields and the background flow fields are independent. However, regions of flow blocking, that is, where the total horizontal wind speed is zero, can be identified. For example, Hines (1988) shows that for a homogeneous flow over a bell-shaped ridge the blocking condition is $F \leq F_c = 0.5$, where F_c is the critical Froude number at which the flow first becomes statically unstable at some point. On the basis of laboratory experiments in a salt-stratified water channel, Rottman and Smith (1989) conclude that for all naturally occurring ridges with aspect ratios less than 0.16, $F_c = 1.0$. This value is twice as great as Hines' value, and this suggests that the linear model underestimates the occurrences of flow blocking. Hines (1988) and Rottman and Smith (1989) studied homogeneous flows; the presence of height varying winds and ambient critical levels will lead to different results.

Figure 8 shows a series of flow "solution" lines above a ridge as the upper-level wind speed is reduced from 4 to -1 m s^{-1} with U_B constant at 4 m s^{-1}. These lines are given by

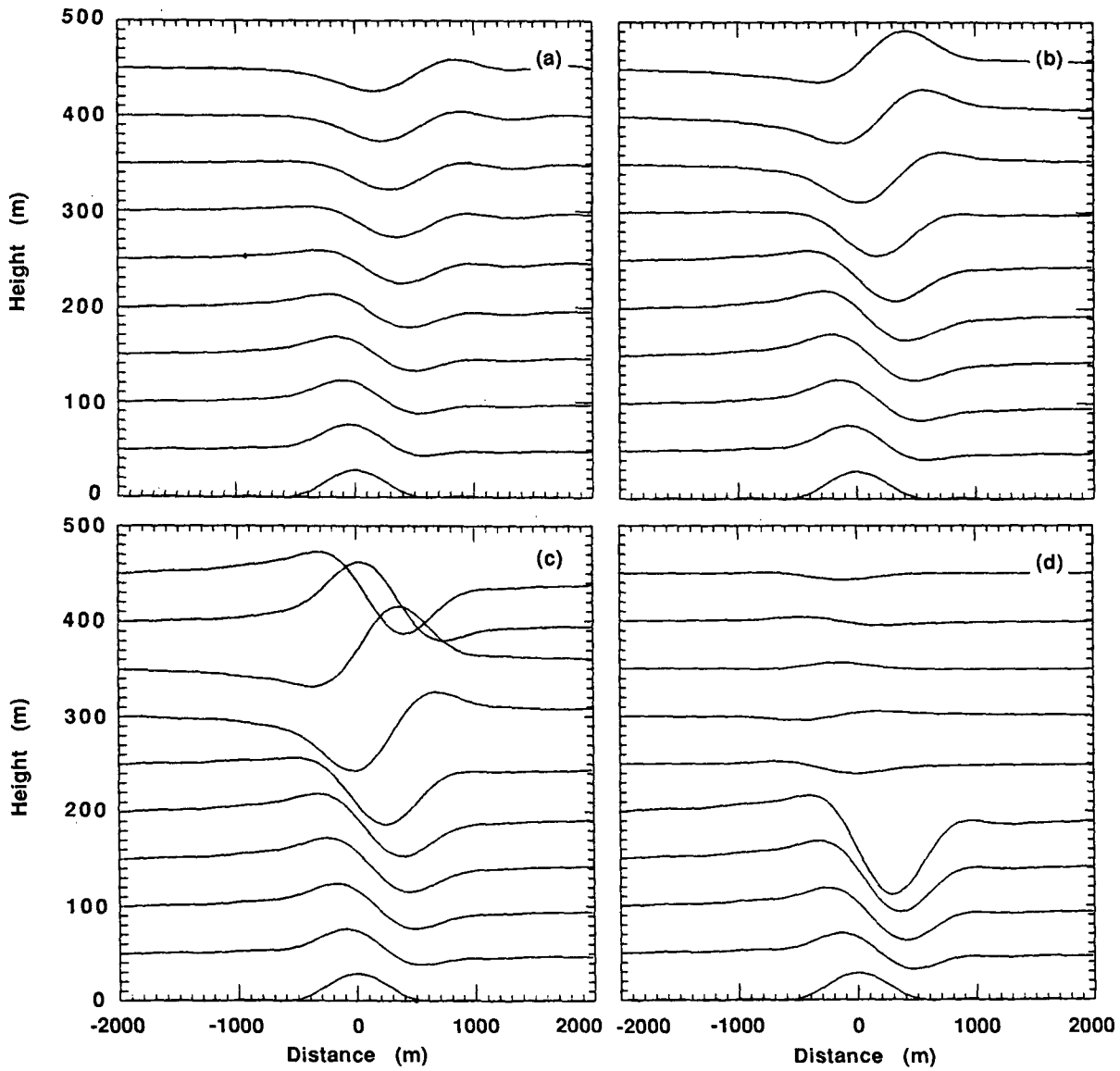

FIG. 8. Solutions lines above a two-dimensional Gaussian ridge; $H = 30$ m, $b = 300$ m, $U_B = 4$ m s^{-1}, and $N = 0.03$ s^{-1}. (a) $U_T = 4$ m s^{-1}, (b) 2 m s^{-1}, (c) 1 m s^{-1}, and (d) -1 m s^{-1}.

$$\eta_s(x, z) = z + \frac{1}{U(z)} \int_{-L}^{x} w(x, z)dx. \quad (3.5)$$

The streamline originating at $z = 0$ far upstream represents the ridge height profile. For the case shown in Fig. 8, the aspect ratio is 0.12, and for the vertically uniform wind case (Fig. 8a) the Froude number is 4.4, which is well above the value of F_c; we can assume that blocking does not occur. Above the ridge the streamlines are somewhat regularly spaced and wave amplitude decreases with height. When U_T is reduced to 2 m s^{-1} (Fig. 8b), the streamline perturbations shift upwind and become more aligned above the ridge. Now wave amplitude increases with height, and the streamlines above about 300 m steepen. When U_T is further reduced to 1 m s^{-1} (Fig. 8c), the lines above 300 m cross. In this case, these lines are no longer streamlines. We take this behavior to be symptomatic of the break-

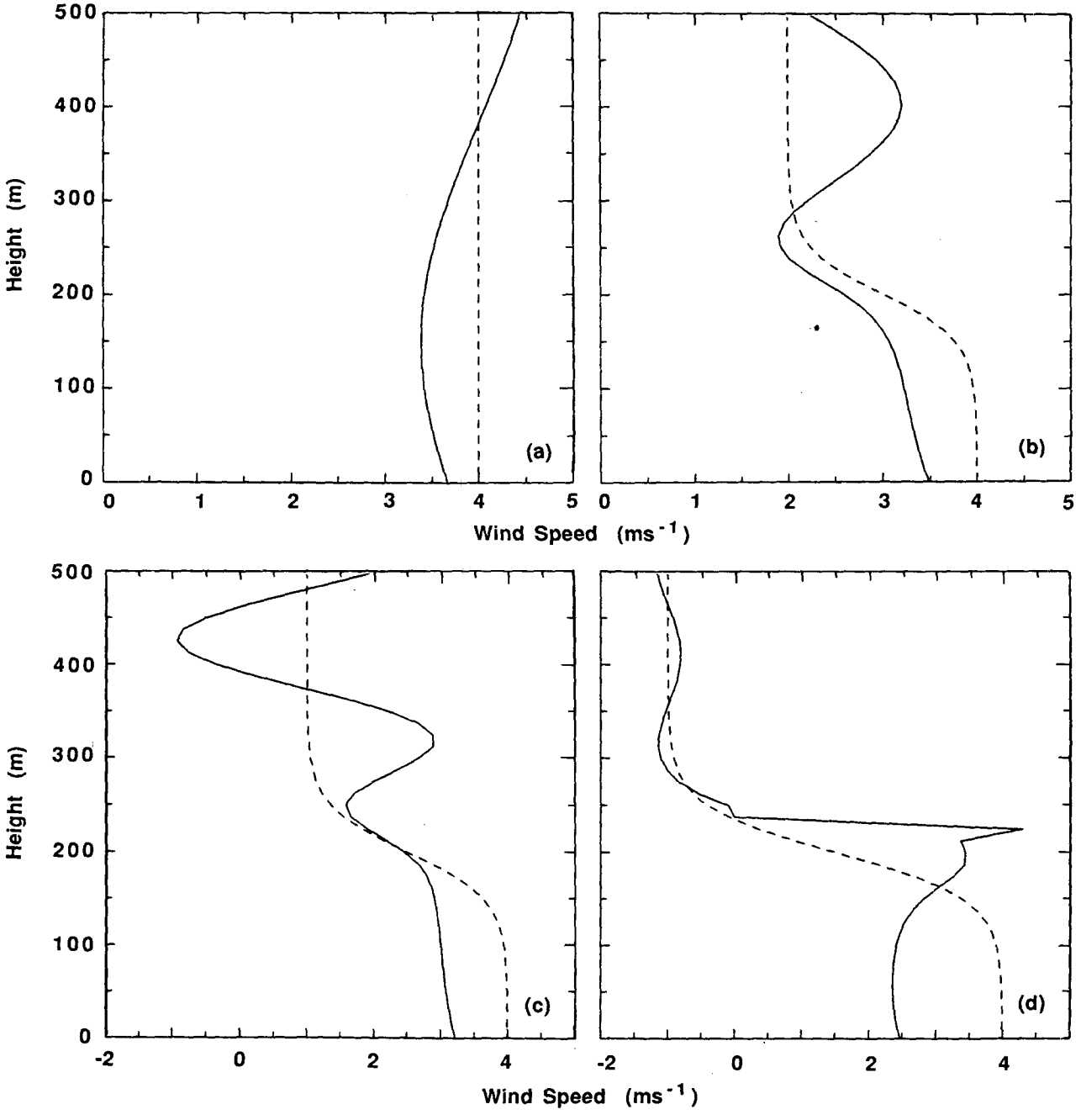

FIG. 9. Profiles of background wind speed (dashed) and total wind speed (solid) at $x = -b/\sqrt{2}$ for the flow fields presented in Fig. 8.

down of the linear wave theory; that is, the vertical displacements, η_s, become very large. In these regions, flow blocking and wave breaking can be anticipated. When $U_T = -1$ m s^{-1}, a critical level exists at a height of about 245 m. Although not shown in Fig. 8d, the lines originating between 200 and 250 m cross and have amplitudes that exceed the scale of the graph.

Profiles of the background and total wind speed for the four cases in Fig. 8 are plotted in Fig. 9. These profiles are taken at the point $x = -b/\sqrt{2}$, which is where the horizontal wave velocity will have a maximum negative value and where flow reversals will first occur. For the uniform wind case (Fig. 9a), the vertical variation of the wave perturbation horizontal velocity is approximately equal to the hydrostatic wavelength $2\pi U/N$, that is, 840 m. As the velocity shear increases, so does the complexity of the total flow. When $U_T = 1$ m s^{-1} (Fig. 9c), the total flow first reverses its direction at about 380 m. From Fig. 8c, it is seen that the solution lines (3.4) originating near these heights intersect, indicating a breakdown of the linear theory. The vertical wavelength of the perturbation in the upper-half space

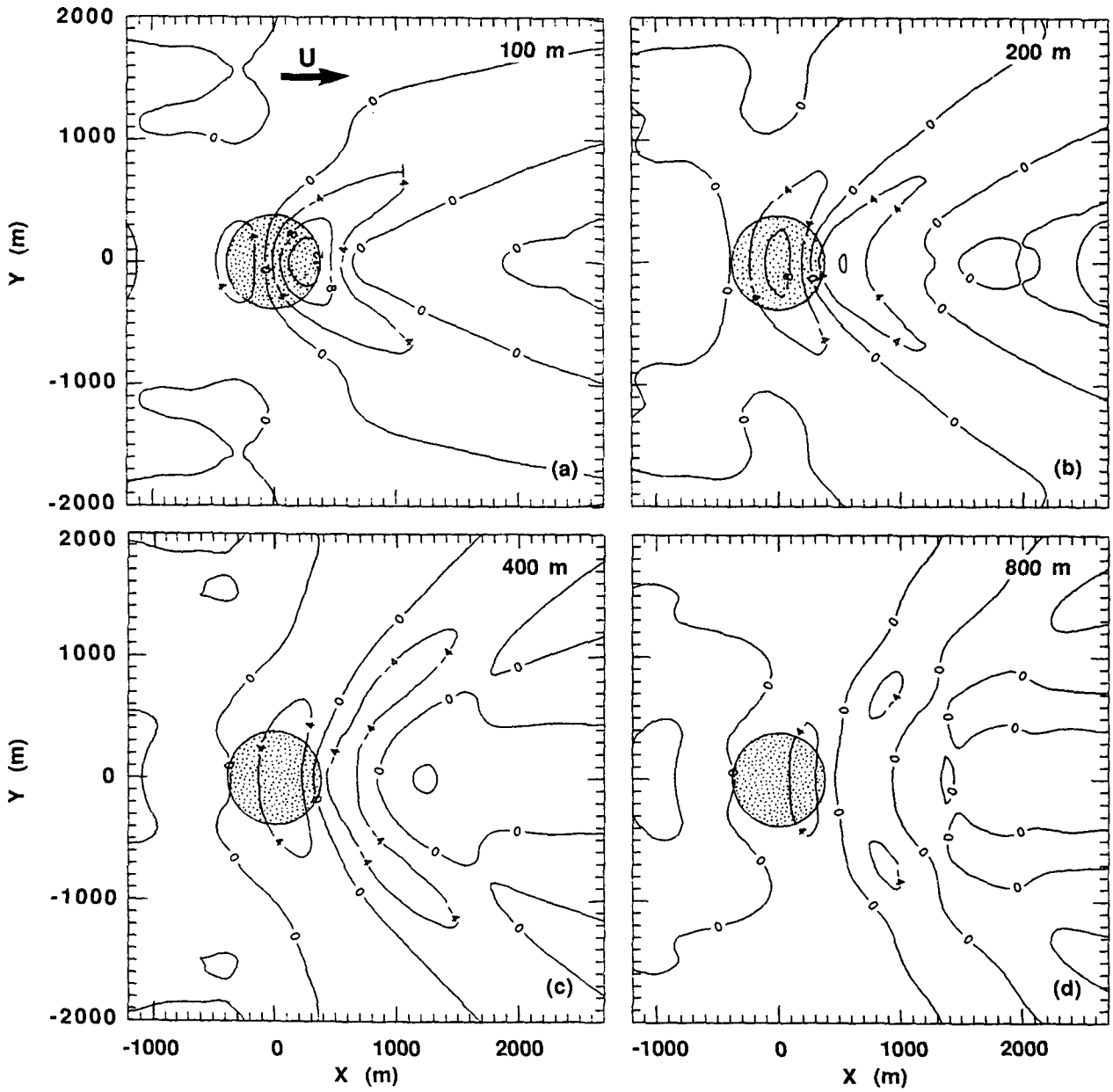

FIG. 10. Vertical displacements of flow streamlines above a three-dimensional Gaussian-shaped hill in the absence of wind shear; $H_G = 30$ m, $b = 300$ m, $N = 0.03$ s^{-1}, and $U_T = U_B = 2$ m s^{-1}.

is about 210 m, which equals the hydrostatic wavelength in that region. Flow reversals are predicted to occur at vertical intervals of about 100 m. When an ambient critical level is present, as in Fig. 9d, the wave amplitudes are greatly reduced above the critical level so that higher altitude flow reversals are not created.

c. *Three-dimensional case*

1) THE FLOW FIELDS

Figure 10 shows the horizontal fields of streamline displacements at various heights above a Gaussian-shaped hill. The hill is centered on the origin of the coordinates, and the shaded circle represents the area contained within the height contour $h = 0.2H_G$. For this case, the Froude number is 2 and $Nb/U = 4.5$. The streamline patterns in Fig. 10 are quite similar to those found in Smith (1980) and Lin (1986), even though those studies were based on a tropospheric scaling. It should be noted that Lin (1986) examined the flow perturbations caused by a three-dimensional heat source, not a mountain. The flow streamline displacements in the x–z plane at $y = 0$ are shown in Fig. 11. These streamlines are also quite similar to those seen in Fig. 5 of Smith (1980). Wave amplitude decreases with height above the hill because of the horizontal spreading of the disturbance field. The introduction of a noncritical wind shear changes the flow fields, but these are not significantly great changes. Over reasonable differences between U_T and U_B, the streamline displacements very much resemble those shown in Figs. 10 and 11. However, the flow field is significantly changed when a critical level is introduced.

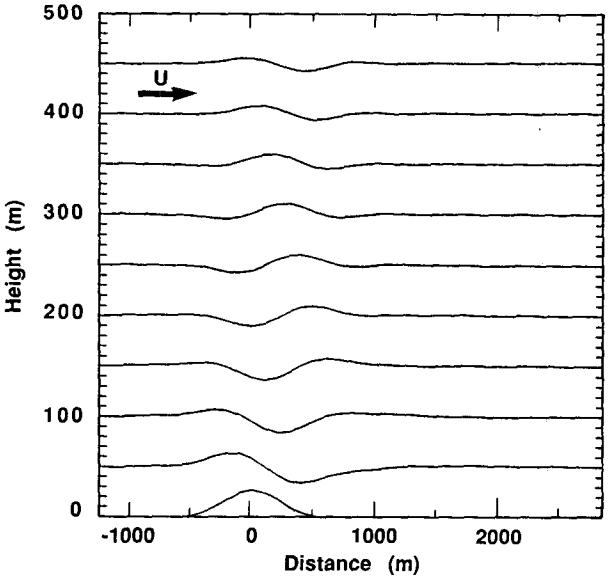

FIG. 11. Vertical displacements of flow streamlines above a three-dimensional Gaussian-shaped hill in the x–z plane at $y = 0$ for the flow field in Fig. 10.

Figure 12 shows the horizontal fields of the vertical displacements when a critical level is present. In this case, $U_T = -1$ m s^{-1} and $U_B = 4$ m s^{-1}. The critical level is at $z = 235$ m; the Richardson number there is about 0.5. The flow disturbances now tend to remain concentrated above the hill rather than spread out away from the hill. At the first model level above the critical level, $z = 250$ m, the amplitudes of the wave disturbances are reduced by about a factor of 10. The streamline displacements in the x–z plane at $y = 0$ are shown in Fig. 13. It is clear that the wave absorption across the critical level is essentially complete. It is also seen in Fig. 13 that below the critical level, the wave amplitude grows with height above the hill. Just as in the two-dimensional case, the wave disturbances become extremely large as the critical level is approached. In these cases, flow blocking can be expected.

2) WAVE DRAG

When a stable flow is directed over an isotropic hill, as in the present case, the Reynolds stresses in the crosswind direction, τ_y, will be antisymmetric. In this case, their contributions to the wave drag will cancel so that the total wave drag is given by

$$D_H = -\bar{\rho}\int_{-\infty}^{\infty}\int_{-\infty}^{\infty} u(x, y, 0)w(x, y, 0)dxdy. \quad (3.6)$$

The average Reynolds stress, $\tilde{\tau}$, over the hill is obtained by dividing D_H by the horizontal cross-sectional area of the hill, which we take to be the area enclosed by the height contour line $h = 0.2H_G$ (Hines 1988). For an isotropic Gaussian hill, this area is $5.06b^2$. Sample curves of average Reynolds stress, normalized by H_G^2 as functions of U_T, are shown in Fig. 14. Comparison of these curves with corresponding curves in Fig. 3 shows that the average drag over a three-dimensional hill is about half of that over a two-dimensional ridge. This is in agreement with the results of Blumen and McGregor (1976), which are based on a hydrostatic flow and tropospheric scaling. The comparison of Fig. 14 with Fig. 3 also shows that the variations of average stress with wind speed over two- and three-dimensional obstacles are similar.

3) WAVE-GENERATED VORTICITY

In section 2c, we demonstrated that the horizontal variations of τ_x and τ_y, defined in (2.15), generate a perturbation vorticity when they are absorbed into the mean flow near a critical level. Figure 15 shows the spatial distributions of the stress couple s, defined in (2.21), when a critical level is present. If the dissipation distance δ, in (2.24), is 50 m, and if $s = 5000 \times 10^{-6}$ N m^{-3}, then $\zeta = 8 \times 10^{-6}(t - t_0)$ s^{-1}. For comparison, the vorticity at midlatitudes due to the earth's rotation is about 10^{-4} s^{-1}. Thus, within a few minutes time, the gravity-wave-generated vorticity will exceed this

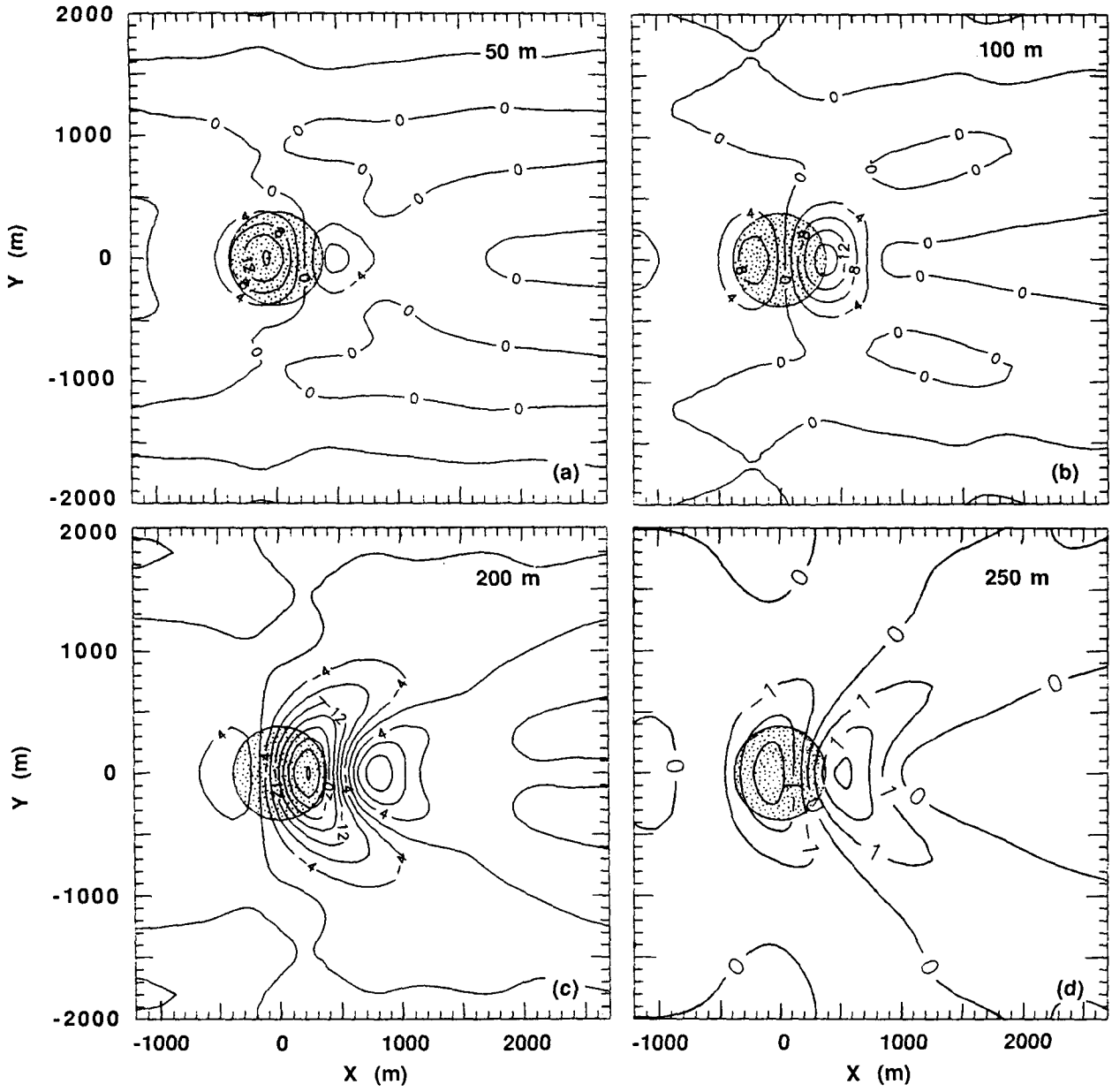

FIG. 12. As in Fig. 10 but with $U_T = -1$ m s^{-1} and $U_B = 4$ m s^{-1}.

value. The horizontal contours of this vorticity will be essentially identical to the contours shown in Fig. 15b. We expect that these vortices will form standing eddies above the hill much like whirlpools in a stream but that the intensities of their circulations will increase with time until other effects stabilize their amplitudes or until the system breaks down.

Vortices in the lee of three-dimensional hills have been observed in laboratory flows by Hunt and Snyder (1980) and in nonlinear, nonhydrostatic model calculations by Smolarkiewicz and Rotunno (1989). Hunt and Snyder's (1980) results show that the lee vortices occur in conjunction with flow separation at Froude numbers below 1.7. Smolarkiewicz and Rotunno (1989) performed inviscid flow simulations and showed that the lee vortices occur for values of Froude number less than 0.5. Their use of a free-slip bottom boundary condition precludes the generation of horizontal vorticity in the boundary layer and subsequent tilting into the vertical direction. They argue that the lee vortices are generated by the tilting of the horizontal vorticity created through baroclinic production as the isentropes bend upward, and subsequently downward, as the flow passes over the obstacle. Smith (1989) offers

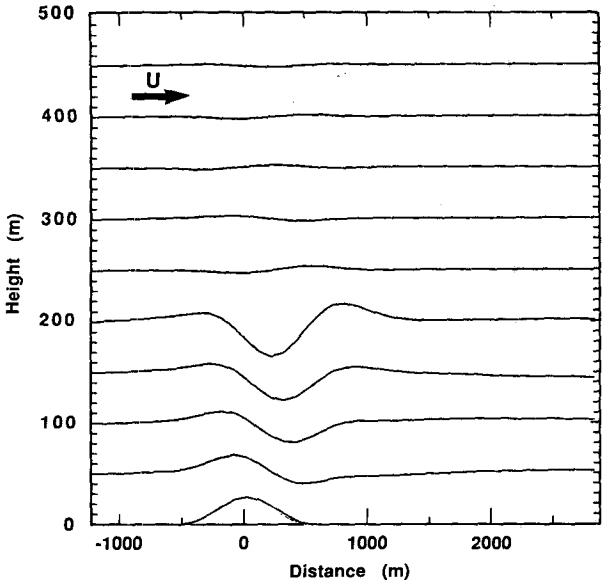

FIG. 13. As in Fig. 11 but with $U_T = -1$ m s^{-1} and $U_B = 4$ m s^{-1}.

a different explanation. However, whatever the cause of the vortices observed in Smolarkiewicz and Rotunno (1989), it is not clear what role, if any, gravity waves play; at such low values of Froude number it is certain that the linear theory is not valid.

Our calculations do not predict vorticity in the flow field. This is beyond the linear theory. Rather, we predict a potential for vorticity when wave absorption occurs near a critical level. This mechanism is not limited to low Froude number flows and is therefore a process quite different than those proposed by either Smolarkiewicz and Rotunno (1989) or Smith (1989).

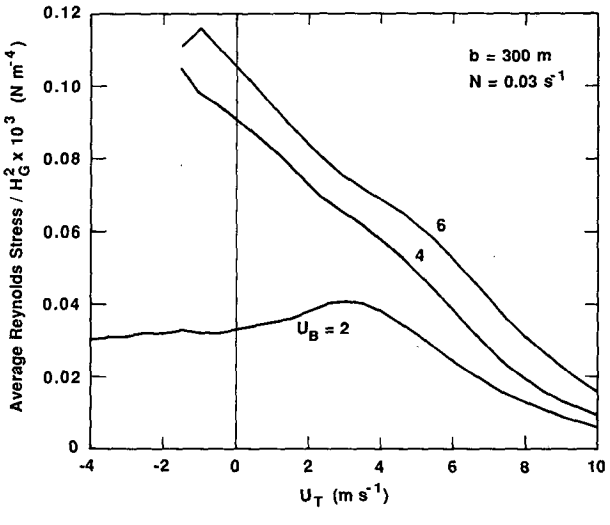

FIG. 14. Average Reynolds stress above a three-dimensional Gaussian-shaped hill as a function of upper-level wind speed. Values are normalized by the square of the maximum hill height; $N = 0.03$ s^{-1} and $b = 300$ m.

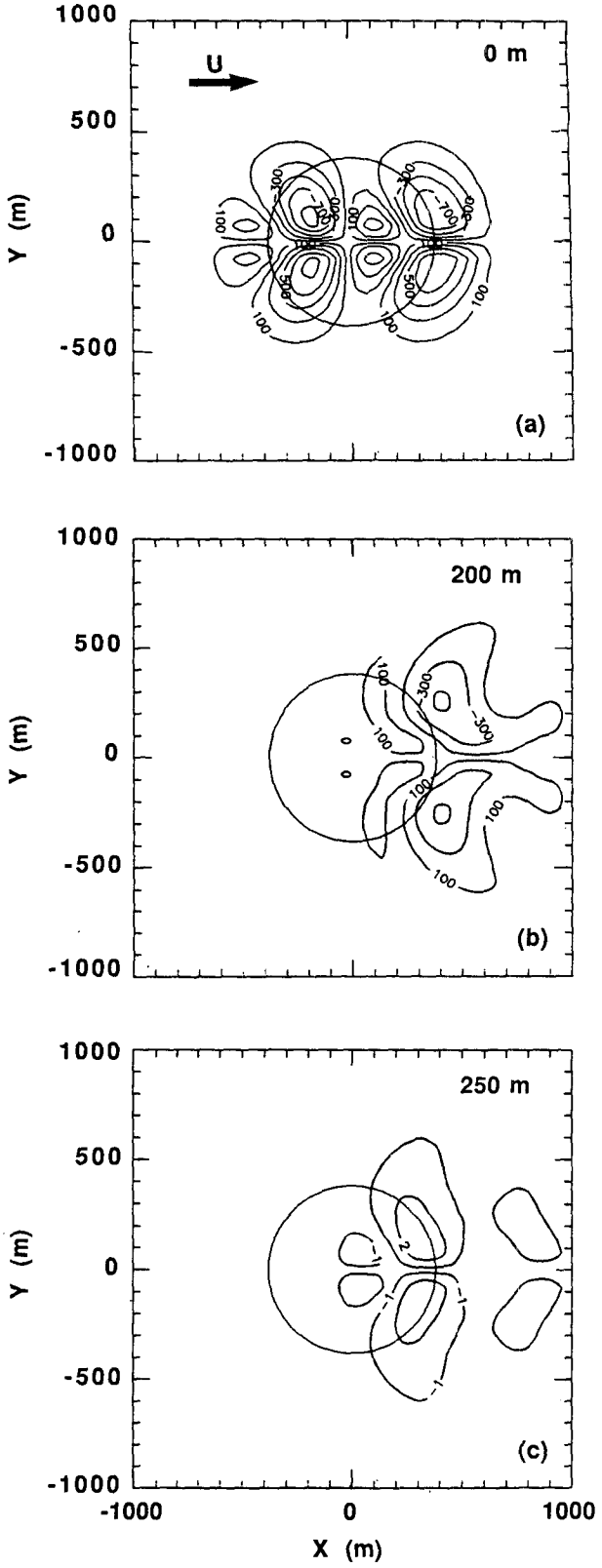

FIG. 15. Stress couples 5×10^6 (N m^{-3}) when a critical level is present; $U_B = 4$ m s^{-1}, $U_T = -1$ m s^{-1}, $H_G = 30$ m, $b = 300$ m, and $z_c = 235$ m.

4. Concluding remarks

The results of this analysis suggest that surface-generated internal gravity waves are quite common in the stable PBL. We have also seen that in regions of rough terrain, where wave generation is most likely, large wind-direction shears and flow reversals produce critical levels for these waves. This has two immediate consequences. First, it presents a dynamic not yet accounted for in conventional PBL theory; second, it offers a means of observing this "mountain wave" phenomenon close to the ground surface where measurements can be made more easily than at higher elevations of the atmosphere.

Conventional PBL theory assumes that the upper levels of the stable layer do not directly sense the ground surface, and gravity waves are not taken into account. Further, it is commonly assumed that the stable stratification always acts to keep turbulence levels low and that turbulence decreases monotonically with distance away from the ground surface. However, beginning with the early observations by Durst (1933), Gifford (1952), and Lyons et al. (1964) and later by, for example, Bean et al. (1973), Kondo et al. (1978), Mahrt (1985), and Gossard et al. (1985), it is now clear that sporadic outbreaks of turbulence, that is, breakdowns of the PBL structure, are common. Recently Nappo (1991) performed a climatological study of these breakdown events over simple and complex terrain. He concludes that a major portion of the nighttime exchange of heat, momentum, and atmospheric pollutants between the atmosphere and the ground surface occurs during these breakdowns, and that the statistics of these events are essentially the same over urban, rural, and complex terrain environments. It is quite possible that these breakdowns are manifestations of wave-turbulence interactions near PBL critical levels.

The linear theory predicts a reduction of Reynolds stress as a gravity wave passes through a critical level. However, exactly what happens there is unknown. Numerical experiments using nonlinear hydrodynamic models predict strong wave reflection at a critical level, while wave saturation theory predicts a partial but continuous reduction of energy as the wave approaches a critical level. These theoretical investigations have been limited to the upper atmosphere where wave amplitudes are large. However, this region of the atmosphere is not generally accessible for observation. Except for a difference in scaling, wave processes in the PBL and the upper atmosphere are expected to be identical. Indeed, the studies of wave–turbulence interactions made by, for example, Einaudi and Finnigan (1981) and Finnigan (1988) are based on measurements made in the surface layer, and there is nothing that would limit their results to the boundary layer. Continuous measurements of wind speed, wind direction, turbulence, and wave activity throughout the depth of the boundary layer are now possible using doppler sodar (for example, see Coulter 1990; Neff 1986); more sensitive measurements using sonic anemometers can be made on tall towers such as that at Boulder, Colorado.

We have demonstrated that even mild perturbations in surface height can launch internal gravity waves and that the surface stress associated with these waves can be larger than the friction stress. At a boundary-layer critical level, we predict that the wave drag will act on the mean flow, generating discrete regions of turbulence. Patches of turbulence, as well as intermittent breakdowns of the PBL stratification, have been observed; we speculate that these events are consistent with surface-generated gravity wave interactions with boundary-layer critical levels. Our calculations show that the average wave stress over a three-dimensional hill is about half that over a two-dimensional ridge of similar height and width. A new result is the prediction of counterrotating vortices in the lee of a three-dimensional isotropic hill near a critical level, where the wave stresses act on the mean flow. Our investigations show that wave processes in the PBL are not different from similar processes in the upper atmosphere. However, these processes can be more easily observed in the PBL.

Acknowledgments. This research was funded in part by an agreement between the National Oceanic and Atmospheric Administration and the U.S. Department of Energy. It was supported in part by the National Science Foundation under Grant ATM-8804623. We thank Mrs. Ann Houston for her skillful typing of this manuscript.

APPENDIX

Analytical Treatment of the Critical Level

A brief description of the analytical solution of the Taylor–Goldstein equation across a critical level is presented. We begin by expanding $U(z)$ in (2.1) to second order in a Taylor series about z_c. This results in

$$\hat{w}_{zz} + \left[\frac{R_c}{\eta^2} - \frac{a_2}{a_1\eta}(R_c + 1) + \gamma\right]\hat{w} = 0, \quad \text{(A.1)}$$

where

$$a_1 = \left.\frac{\partial U}{\partial z}\right|_{z_c}, \quad a_2 = \left.\frac{\partial^2 U}{\partial z^2}\right|_{z_c}, \quad \eta = z - z_c,$$

$$\gamma = \frac{1}{2}(a_2/a_1)^2 - k^2, \quad R_c = N^2/a_1^2. \quad \text{(A.2)}$$

Then $\hat{w}$ is expressed by the Frobenious expansion

$$\hat{w}(k, z_c + \eta) = \sum_n C_n \eta^{n+\lambda}. \quad \text{(A.3)}$$

Using (A.3) in (A.1) leads to recursion relations for the expansion coefficients, that is,

$$C_1 = \frac{(a_2/a_1)(R_c + 1)}{\lambda(\lambda + 1) + R_c} C_0 \quad \text{(A.4)}$$

$$C_2 = \frac{C_1 + \gamma C_0}{(\lambda + 1)(\lambda + 2) + R_c}. \quad \text{(A.5)}$$

The expansion parameter λ is found to be

$$\lambda = \frac{1}{2} \pm i[R_c - 0.25]^{1/2}. \quad \text{(A.6)}$$

Equation (A.3) can be expanded to get

$$\hat{w}(k, z_c + \eta) = C_0^+ \eta^\lambda A(\eta) + C_0^- \eta^{\lambda^*} A^*(\eta), \quad \text{(A.7)}$$

where

$$A(\eta) = 1 + \frac{C_1}{C_0}\eta + \frac{C_2}{C_0}\eta^2 \quad \text{(A.8)}$$

and the asterisk denotes the complex conjugate value. To evaluate the complex constants C_0^+ and C_0^-, we first take the vertical derivative of (A.7) to get

$$\frac{d\hat{w}}{dz} = C_0^+ \eta^\lambda B(\eta) + C_0^- \eta^{\lambda^*} B^*(\eta), \quad \text{(A.9)}$$

where

$$B(\eta) = \lambda\eta^{-1} + \frac{C_1}{C_0}(\lambda + 1) + \frac{C_2}{C_0}(\lambda + 2)\eta. \quad \text{(A.10)}$$

Then using (A.7) and (A.9), one gets

$$C_0^+ = (A^* d\hat{w}/dz - B^*\hat{w})/D \quad \text{(A.11)}$$

$$C_0^- = (A d\hat{w}/dz - B\hat{w})/D^*, \quad \text{(A.12)}$$

where

$$D = A^*B - AB^*. \quad \text{(A.13)}$$

At distance η below z_c, (A.7) and (A.9) become

$$\hat{w}(k, z_c - \eta) = C_0^+(-1)^\lambda \eta^\lambda A(-\eta) + C_0^-(-1)^{\lambda^*} A^*(-\eta) \quad \text{(A.14)}$$

and

$$\frac{d\hat{w}}{dz}(k, z_c - \eta) = -C_0^+(-1)^\lambda \eta^\lambda B(-\eta) + C_0^-(-1)^{\lambda^*} \eta^{\lambda^*} B^*(-\eta), \quad \text{(A.15)}$$

respectively. Before (A.14) and (A.15) can be evaluated, we must know how to express -1 in complex form. Booker and Bretherton (1967) show that

$$-1 = e^{-i\pi} \left.\frac{dU}{dz}\right|_{z_c} > 0 \quad \text{(A.16)}$$

$$-1 = e^{i\pi} \left.\frac{dU}{dz}\right|_{z_c} < 0. \quad \text{(A.17)}$$

In the model, $\hat{w}$ and $d\hat{w}/dz$ are solved numerically from the upper boundary to height $z_c + \eta$, where C_0^+ and C_0^- are evaluated using (A.11) and (A.12). Below the critical level, $\hat{w}(k, z_c - \eta)$ and $d\hat{w}/dz(k, z_c - \eta)$ are obtained from (A.14) and (A.15), respectively. The numerical solutions continue from this point downward to the ground surface.

REFERENCES

Bachmeister, J. T., and R. T. Pierrehumbert, 1988: On high-drag states of nonlinear stratified flow over an obstacle. *J. Atmos. Sci.*, **45**, 63–80.

Bean, B. R., A. S. Frisch, L. G. McAllister, and J. R. Pollard, 1973: Planetary boundary-layer turbulence studies from acoustic echo sounder and in situ measurements. *Bound.-Layer Meteor.*, **4**, 449–474.

Blumen, W., 1965: Momentum flux by mountain waves in a stratified rotating atmosphere. *J. Atmos. Sci.*, **22**, 529–534.

——, and C. D. McGregor, 1976: Wave drag by three-dimensional lee-waves in nonplanar shear flows. *Tellus*, **28**, 287–298.

Booker, J. R., and F. P. Bretherton, 1967: The critical level for internal gravity waves in a shear flow. *J. Fluid Mech.*, **27**, 513–539.

Bretherton, F. P., 1969: Momentum transport by gravity waves. *Quart. J. Roy. Meteor. Soc.*, **95**, 213–243.

Brost, R. A., and J. C. Wyngaard, 1978: A model study of the stably stratified planetary boundary layer. *J. Atmos. Sci.*, **35**, 1427–1440.

Businger, J. A., J. C. Wyngaard, Y. Izumi, and E. F. Bradley, 1971: Flux-profile relationships in the atmospheric surface layer. *J. Atmos. Sci.*, **28**, 181–189.

Chimonas, G., and C. O. Hines, 1986: Doppler ducting of atmospheric gravity waves. *J. Geophys. Res.*, **91**, 1219–1230.

——, and C. J. Nappo, 1987: A thunderstorm bow wave. *J. Atmos. Sci.*, **44**, 533–541.

——, and ——, 1989: Wave drag in the planetary boundary layer over complex terrain. *Bound.-Layer Meteor.*, **47**, 217–232.

Clark, T. L., and W. R. Peltier, 1977: On the evolution and stability of finite-amplitude mountain waves. *J. Atmos. Sci.*, **34**, 1715–1730.

Clarke, R. H., A. J. Dyer, R. R. Brook, D. G. Reid, and A. J. Troup, 1971: The Wangara experiment: Boundary layer data. Div. Meteor. Phys. Tech. Pap. No. 19, CSIRO.

Clements, W. E., J. A. Archuleta, and D. E. Hoard, 1989: Mean structure of the nocturnal drainage flow in a deep valley. *J. Appl. Meteor.*, **28**, 457–462.

Coulter, R., 1990: A case study of turbulence in the stable boundary layer. *Bound.-Layer Meteor.*, **52**, 75–91.

Craik, A. D. D., 1985: *Wave Interactions and Turbulent Flows.* Cambridge University Press, 322 pp.

Delage, Y., 1974: A numerical study of the nocturnal atmospheric boundary layer. *Quart. J. Roy. Meteor. Soc.*, **100**, 351–364.

Durran, D. R., 1986: Another look at downslope windstorms. Part 1: The development of analogs in supercritical flow in an infinitely deep, continuously stratified fluid. *J. Atmos. Sci.*, **43**, 2527–2543.

Durst, C. S., 1933: The breakdown of steep wind gradients in inversions. *Quart. J. Roy. Meteor. Soc.*, **54**, 131–136.

Eliassen, A., and E. Palm, 1960: On the transfer of energy in stationary mountain waves. *Geofys. Publ.*, **22**, 1–23.

Einaudi, F., and J. J. Finnigan, 1981: The interaction between an internal gravity wave and the planetary boundary layer. Part 1: The linear analysis. *Quart. J. Roy. Meteor. Soc.*, **107**, 793–806.

Finnigan, J. J., 1988: Kinetic energy transfer between internal gravity waves and turbulence. *J. Atmos. Sci.*, **45**, 486–505.

Garratt, J. R., 1983: Surface influence upon vertical profiles in the nocturnal boundary layer. *Bound.-Layer Meteor.*, **26**, 69–80.

Gifford, F. A., 1952: The breakdown of a low-level inversion studied by means of detailed soundings with a modified radiosonde. *Bull. Amer. Meteor. Soc.*, **33**, 373–379.

Gossard, E. E., and W. H. Hooke, 1975: *Waves in the Atmosphere.* Elsevier, 456 pp.

——, J. E. Gayner, R. J. Zamora, and W. D. Neff, 1985: Finestructure of elevated stable layers observed by sounder and in situ tower sensors. *J. Atmos. Sci.*, **42,** 2156–2169.

Hines, C. O., 1970: Comments on a paper by E. E. Gossard, J. H. Richter, and D. Atlas: Internal waves in the atmosphere from high resolution radar measurements. *J. Geophys. Res.*, **75,** 5956–5959.

——, 1988: A modeling of atmospheric gravity waves and wave drag generated by isotropic and anisotropic terrain. *J. Atmos. Sci.*, **45,** 309–322.

Hootman, B. W., and W. Blumen, 1983: Analysis of nighttime drainage winds in Boulder, Colorado, during 1980. *Mon. Wea. Rev.*, **111,** 1052–1061.

Hunt, J. C. R., and W. H. Snyder, 1980: Experiments on stably and neutrally stratified flow over a model three-dimensional hill. *J. Fluid Mech.*, **96,** 671–704.

Izumi, Y., and J. R. Caughey, 1973: Minnesota 1973 atmospheric boundary layer experiment data report. Air Force Cambridge Research Laboratory, Meteor. Lab. Rep. No. AFCRL-TR-76-0038, 28 pp.

Kondo, J., O. Kanechika, and N. Yasuda, 1978: Heat and momentum transfer under strong stability in the atmospheric surface layer. *J. Atmos. Sci.*, **35,** 1012–1021.

Lalas, D. P., and F. Einaudi, 1976: On the characteristics of gravity waves generated by atmospheric shear layers. *J. Atmos. Sci.*, **33,** 1248–1259.

Lin, Y., 1986: Calculation of air flow over an isolated heat source with applications to the dynamics of V-shaped clouds. *J. Atmos. Sci.*, **43,** 2736–2751.

——, and S. Li, 1988: Three-dimensional response of a shear flow to elevated heating. *J. Atmos. Sci.*, **45,** 2987–3002.

Lyons, R., H. A. Panofsky, and S. Wallaston, 1964: The critical Richardson number and its implications for forecast problems. *J. Appl. Meteor.*, **3,** 136–142.

Mahrt, L., 1985: Vertical structure and turbulence in the very stable boundary layer. *J. Atmos. Sci.*, **42,** 2333–2349.

——, R. C. Heald, D. H. Lenshow, B. B. Stankov, and I. Troen, 1979: An observational study of the structure of the nocturnal boundary layer. *Bound.-Layer Meteor.*, **17,** 247–264.

Miles, J. W., 1961: On the stability of heterogeneous shear flow. *J. Fluid Mech.*, **10,** 496–508.

Nappo, C. J., 1989: A theoretical investigation of gravity-wave-generated stress and vorticity in the planetary boundary layer. Ph.D. thesis. Georgia Institute of Technology, Atlanta, 176 pp.

——, 1990: Sporadic breakdowns of stability in the PBL over simple and complex terrain. *Bound.-Layer Meteor.*, **54,** 69–87.

Neff, W. D., 1986: On the use of sodars to study stably stratified flow influenced by terrain. *Atmos. Res.*, **20,** 279–308.

Nieuwstadt, F. T. M., 1984: Some aspects of the turbulent stable boundary layer. *Bound.-Layer Meteor.*, **30,** 31–38.

Peltier, W. R., and T. L. Clark, 1979: The evolution and stability of finite-amplitude mountain waves. Part II: Surface wave drag and severe downslope windstorms. *J. Atmos. Sci.*, **36,** 1498–1529.

Rao, K. S., and H. F. Snodgrass, 1979: Some parameterizations of the nocturnal planetary boundary layer. *Bound.-Layer Meteor.*, **17,** 15–28.

Rottman, J. W., and R. B. Smith, 1989: A laboratory model of severe downslope winds. *Tellus,* **41A,** 401–415.

Sawyer, J. S., 1959: The introduction of the effects of topography into methods of numerical forecasting. *Quart. J. Roy. Meteor. Soc.*, **85,** 31–43.

Simard, A., and W. R. Peltier, 1982: Ship waves in the lee of isolated topography. *J. Atmos. Sci.*, **39,** 587–609.

Smith, R. B., 1979: The influence of mountains on the atmosphere. *Adv. Geophys.*, **21,** 87–230.

——, 1980: Linear theory of stratified hydrostatic flow past an isolated mountain. *Tellus,* **32,** 348–364.

——, 1989: Comment on "Low Froude number flow past three-dimensional obstacles. Part I: Baroclinically generated lee vortices." *J. Atmos. Sci.*, **46,** 3611–3613.

Smolarkiewicz, P. K., and R. Rotunno, 1989: Low Froude number flow past three-dimensional obstacles. Part 1: Baroclinically generated lee vortices. *J. Atmos. Sci.*, **46,** 1154–1164.

Wyngaard, J. C., 1975: Modeling the planetary boundary layer—extension to the stable case. *Bound.-Layer Meteor.*, **9,** 441–460.

Yamamoto, S., O. Yokoyama, and M. Gamo, 1979: Observational study on the turbulent structure of the atmospheric boundary layer under stable conditions. *J. Meteor. Soc. Japan,* **57,** 423–431.